JOURNAL OF CATALYSIS **167,** 12–24 (1997)
ARTICLE NO. CA971563

Morphology and Crystallographic Relationships in Reduced Magnetite: A Comprehensive Structural Study of the Porous Iron Ammonia Synthesis Catalyst

Børge Holme

Department of Physics, University of Oslo, P.O. Box 1048 Blindern, N-0316 Oslo, Norway

Received October 16, 1995; revised October 4, 1996; accepted November 28, 1996

Ammonia synthesis catalyst has been examined by optical microscopy and transmission electron microscopy. In reduced magnetite grains four different pore morphologies with characteristic crystallographic orientations exist. These structures are several micrometers in size and may be described as porous single crystals of bcc-iron. The dominant structure (roughly 80% of the catalyst volume) contains a nearly random network of pores and the crystallographic orientation of the porous iron is the same as that of the original magnetite. Another structure (ca. 5% by volume) has sheets of iron along the three {100} **planes of the former magnetite and a** ⟨100⟩ **axis of iron normal to the sheets. A third structure (ca. 3%) with weakly sheet-like pores along the twelve** {112} **planes of the original magnetite has a** ⟨221⟩ **direction of iron normal to the pores. The most complex structure (very rare in the industrial catalyst) displays strongly sheet-like pores along the four** {111} **planes of magnetite and has a** ⟨100⟩ **axis of iron normal to the sheets. The particular orientation relations between the original magnetite and the resulting iron suggests that epitaxy plays an important role during reduction. Alumina, which is added as a promoter, reduces the lattice parameter of magnetite. The local Al^{3+} concentration in the magnetite may influence which structure occurs by changing the likelihood of the possible epitaxy relations. Differences in activity among the various structures may exist. However, activity measurements are not a part of this structural study of the porous iron ammonia synthesis catalyst.**

INTRODUCTION

It has been known for a long time that the industrial ammonia synthesis catalyst is a very inhomogeneous system. In an optical microscope one can easily see the outline of magnetite, wüstite, and other phases. We present here a comprehensive study of the structures and phases present in the ammonia synthesis catalyst. Our main purpose is to show that *within* the reduced magnetite grains there is a wide variety of pore structures with systematic crystallographic orientations of the porous iron. These structures become clearly visible in polarized light microscopy. We have used optical microscopy on specimens prepared for transmission electron microscopy (TEM) to find the relations between pore geometry and the crystallographic orientations of the porous iron. In this way it was possible to study the catalyst on length scales ranging from nanometers to millimeters.

Triply promoted ammonia synthesis catalyst is prepared from a melt containing iron oxide and about 2% by weight of aluminum, calcium, and potassium oxide. These added elements function as *promoters*; i.e., they increase the catalytic activity in various ways. After solidification the catalyst consists of magnetite, Fe_3O_4, with dissolved aluminum oxide (1), often a few percent wüstite, $Fe_{1-x}O$, and more complex iron-promoter oxides (2–4) between the magnetite grains.

The active catalyst is produced by reduction of the iron oxides with a hydrogen and nitrogen gas mixture at temperatures in the range 620–800 K. Hydrogen removes oxygen and escapes as water vapour, leaving porous iron and unreduced promoter oxides behind. In addition, the iron surface is partly covered by a spinel phase which can be thought of as magnetite that was enriched in Al^{3+} ions during reduction and thus remained unreduced (5). This $Fe_{3-x}Al_xO_4$ spinel phase has the same crystallographic orientation as the original magnetite and we will refer to it here simply as "magnetite" since we are mostly concerned with orientational relations.

In the subsequent stabilization process the remaining iron surface is oxidized to a thickness of about 2 nm (6).

During reduction the volume of solid matter is halved; thus approximately half of the apparent volume consists of pores. However, the former magnetite grains retain their shape on a micrometer scale and their outline can be seen also in *reduced* specimens.

The bulk properties of the catalyst have been studied extensively in the past, mostly using X-ray diffraction (2, 7), Mössbauer spectroscopy (8–10), and chemisorption techniques (11). Electron microscopy studies have given information about the pore structure and crystallite orientation of the catalyst (3, 12). In a recent paper (13), based on both optical microscopy and transmission electron

0021-9517/97 $25.00

microscopy, one particular pore structure was described in detail.

In the present paper, we describe the pore structure and crystallographic orientation of iron in other kinds of regions found within reduced magnetite grains in the ammonia synthesis catalyst. We further present statistics showing the abundance of the various structures in an industrial catalyst. The effect of dissolved alumina in the magnetite phase is mentioned as one of the factors which might control the occurrence of the different structures. Finally, we discuss possible differences in catalytic activity for the various structures.

EXPERIMENTAL

The specimens used in this study were industrial ammonia synthesis catalyst particles of size fraction 6–10 mm from three different manufacturers. We will call them catalysts A, B, and C. All images and statistical results are based on examination of catalyst A. Three samples each of catalysts A, B, and C were reduced together and examined in optical microscopy in order to determine whether the structures described here are a general occurrence. All structures and phases observed in catalysts B and C were also found in catalyst A, indicating that there are mainly quantitative differences in pore structure, iron crystallite orientation and reduction behaviour between catalysts made by different manufacturers.

In the present study we have examined more than 250 individual particles of catalyst A in order to ensure that the results given here are representative and fairly complete.

Most of the magnetite specimens were industrially reduced in a 3 : 1 mixture of H_2 and N_2 before being stabilized. Other specimens were reduced under laboratory conditions, i.e., pure hydrogen gas and temperatures up to 800 K. No qualitative differences were found between industrially and laboratory reduced specimens.

All specimens were prepared for optical microscopy by grinding and polishing according to standard metallographic techniques. Although the specimen preparation might have caused changes in the catalyst surface on the atomic scale, it will be assumed that the nanometer scale pore structure was not altered. This means that the polished sections observed in the optical microscope are considered to be representative for the bulk catalyst. The notion that the pore structure is fairly stable, once it is formed, is supported by several observations. For instance, optical microscope specimens can be repeatedly polished to remove micrometer thick layers, while consistently revealing deeper sections of the same structure in any given magnetite grain. Further, micrographs taken of TEM-specimens at different stages of ion milling show that the pore structures remain, even though the specimen is thinned.

The optical microscope used in this study was a Reichert–Jung MeF 3 metallography microscope with polarizing filters and a 273-nm λ-plate retarder that was traversed twice by the light path. The polarizing filters were in a crossed position and the fast axis of the retarder was at an angle of 6° from the transmission axis of the analyzer. In the mode of operation of the optical microscope used throughout this paper, a region looks yellow if the nanometer scale pore structure of the polished surface has a dominant pore direction along the lower left to upper right diagonal (/) of the images. Similarly, a dominant pore direction along the opposite diagonal (\ ) will make the region appear purple or blue. This is a purely optical effect related to the microscope filter positions; rotating the specimen stage by 90° made blue and yellow regions switch colour.

The microscope was connected to a computerized image analysis system, Vidas 2.5 from Kontron Elektronik. Quantitative measurements of area fractions for the various structures were performed on this system using programs specially made for this purpose. For any system containing a randomly distributed phase in a matrix, the area fraction of that phase in a polished surface is equal to the volume fraction of the bulk specimen (14). We assume throughout that this relationship also holds for the structures in the catalyst. However, the large inhomogeneities among and within particles imply that the sample size in the quantitative analysis should not be too small. We studied 20 randomly selected particles from an industrially prereduced catalyst. Nearly the entire polished surface area of each catalyst particle was examined. The number of pixels covered by a certain structure was found, either through segmentation by colour or by manually tracing out all the regions where one particular structure was present. In this way more than five million pixels were segmented and this should give a relatively reliable estimate for the volume fraction of the more common structures.

We designed a special instrument which enabled us to measure electrical resistance in the polished surfaces of optical microscope specimens. Two sharpened needles could be placed on the specimen surface with a separation of about 40–60 μm while the specimen was studied in an Olympus BX50 geological microscope. We measured the resistance in the specimen surface using a digital Fluke multimeter. Since we knew exactly where the resistance measurement was made, it was possible to obtain values of the resistance within the various structures and phases of the catalyst. The resistance value on the multimeter would generally fluctuate greatly in both time and position even though the needles were placed on the surface with comparable force and separation in each measurement. We choose to discard the readings where the resistance was unusually high or unstable, assuming that surface contamination, oxides, dust, etc. were perturbing the measurements at such places. All samples were cleaned with

cotton soaked in methanol and dried in hot air prior to the measurements.

Transmission electron microscopy was performed on a JEOL 200 CX instrument operated at 200 kV accelerator voltage.

RESULTS

For reasons of easy reference we have given names to the different *structures* encountered within reduced magnetite grains in the catalyst. The names are intended to reflect the appearance of the different structures in the optical microscope. The structure described in Ref. (13) will henceforth be called *Normal Structure*, whereas the other three structures described here are referred to as *Plain Structure*, *Finger Structure*, and *Flake Structure*. Before we describe these structures in detail we will briefly mention some other characteristic features and phases in the catalyst.

Overview of Phases and Structures Based on Optical Microscopy and TEM

The inhomogeneous nature of the ammonia synthesis catalyst is clearly seen in Fig. 1, which shows the many different phases and structures in the catalyst as revealed by polarized light microscopy. The nine images (a–i) are made at various magnifications from different specimens but one single 10 mm catalyst particle could in principle contain all the structures shown here. In most cases, however, one particle tends to contain large amounts of only one or two types of structures.

Dendritic magnetite Figure 1a shows a fully reduced part of the catalyst where the former magnetite grains had long, dendritic shapes quite different from the more common equiaxed grain shape seen in Fig. 1d–g. The large size of dendritic magnetite grains suggests that they were crystallized at a slower cooling rate than the more common equiaxed grains.

Residual magnetite and reduced wüstite. Figure 1b depicts a region with partly reduced magnetite grains on the left hand side and the typical rounded dendrites of wüstite, $Fe_{1-x}O$, at right hand side. The darker, smooth unreduced parts of the grains clearly show the topotactic nature of the reduction process. The reduction gases quickly fill the pores between the compact magnetite grains and then start reducing the magnetite from all sides at nearly the same rate.

When wüstite is present along with magnetite, the wüstite phase is reduced faster than magnetite (8). The activation energy for reduction of wüstite has been found to be roughly half that of magnetite (15). In addition, the wüstite dendrites leave large pores between them where the reduction gases can easily diffuse in and out. Since reduced wüstite has larger pores than reduced magnetite (16–18) and consequently a smaller surface area, it seems that the main positive effect of wüstite in the industrial catalyst is to provide 'highways' where gases can move more easily.

Figure 2 shows a TEM study of a sample containing both reduced wüstite and reduced magnetite. In the bright field image of Fig. 2a the upper left half is reduced magnetite and the lower right half is reduced wüstite. It is clearly seen that the pore structure of reduced wüstite is much coarser than that of reduced magnetite. The selected area diffraction pattern in Fig. 2b was made by centring the aperture on the interface, thus including both kinds of porous iron. The pattern shows a $[135]_{Fe}$ projection from bcc-iron along with a $[135]_m$ projection from magnetite and a ring pattern from polycrystalline iron. The subscript 'm' is used whenever we refer to a direction or a plane in magnetite, whereas the subscript 'Fe' denotes porous bcc-iron.

Selected area diffraction patterns made with the aperture on either side of the interface in Fig. 2a clearly showed that the single crystal [135] projection from iron and magnetite came from the reduced magnetite grain at the upper left, whereas the ring pattern indicating randomly oriented polycrystalline iron came from the reduced wüstite. This result, that magnetite reduces to a structure of great order, while wüstite creates iron crystallites of all orientations, may seem puzzling at first, considering the similarities in the crystal structures of Fe_3O_4 and $Fe_{1-x}O$. However, there may be several reasons for this difference: Since wüstite is not thermodynamically stable below 843 K (570°C) it may disproportionate into magnetite and a wüstite phase of different composition if it is cooled slowly (19), or it may disproportionate to iron and magnetite when heated (4), e.g., in the initial phase of the reduction process. Such disproportionation will result in a rather complex mixture of iron oxides and iron. This could explain one of our observations where we found well ordered iron within a typical rounded wüstite dendrite. The small region could have been reduced from a magnetite crystal made by disproportionation of wüstite. Moreover, as pointed out by Schlögl (4), industrial catalysts may contain large quantities of X-ray amorphous wüstite. Reduction of an amorphous $Fe_{1-x}O$ phase can hardly yield anything but randomly distributed polycrystalline iron, just as we observe.

Needle-shaped oxide phases. Figure 1c shows a cluster of needle-shaped oxides that are partly reduced. Such needles contain promoter-rich iron oxide phases, and several different compositions have been reported in the literature, e.g., $FeAl_2O_4$, $K_2Fe_{22}O_{34}$, and $CaFe_3O_5$ (2, 7, 20). Unreduced regions appear smooth and dark brown in this image. The reduced regions vary in colour from yellow at the left to purple and blue at the lower right. These colours show that the reduced parts of the needles have a pore structure with sheets orthogonal to the needle axis and stacked onto each other like a pile of pancakes. This

morphology has been confirmed by TEM in a previous study (21).

In catalyst particles where all the magnetite is completely reduced, it is not uncommon to find oxide needles that are partly reduced or not reduced at all. These oxides are thus the least reducible component of an industrial catalyst. The needles occur in clusters or individually between magnetite grains or between wüstite dendrites. The positive effect of such needles may be twofold. First, the needles provide a reservoir of potassium, which does not easily dissolve in the magnetite (22), but migrates into the former magnetite grains during reduction (3). Second, the needle-shaped oxides leave large channels between them which facilitate gas transport (18). Thus, the needle-shaped phases in an efficient catalyst should be evenly dispersed throughout the particle and create a connected network of large pores between the magnetite grains.

We now turn to the description of the structures found *within* reduced magnetite grains.

Plain structure. Figure 1d shows the most common of all structures in reduced magnetite grains, constituting about 4/5 of the catalyst volume. We will call it Plain Structure because of its generally plain appearance relative to other, brighter looking structures. In this image we see a distinct hourglass pattern in the central part of four grains. This feature is often present in Plain Structure grains and indicates a dominantly pipe-like pore direction normal to the outer surface of each grain.

We have previously pointed out (13) that magnetite prefers to crystallize as regular octahedra where the $\{111\}_m$ planes form the grain boundaries. We will assume here that this relationship holds and interpret most straight-lined grain boundaries as traces of $\{111\}_m$ planes in the polished surface.

Only in grains with an approximately octahedral shape does the hourglass have such a perfect shape as in Fig. 1d. However, the colours always indicate a preferred direction of pores from the nearest grain surface and orthogonally into the grain along a $\langle 111\rangle_m$ direction of the original magnetite.

Reduced magnetite grains without an hourglass pattern contain a random pore network with no preferred directions. There thus seems to exist a range of pore geometries within the Plain Structure from totally random to quite distinctly along a $\langle 111\rangle_m$ direction.

Figure 3a depicts a reduced magnetite grain containing Plain Structure. At this high magnification the surface looks distinctly speckled since we are on the edge of resolving the pore structure of the catalyst. There is not sign of hourglass structure in this grain. The right edge of the grain is thin enough for TEM examination and the diffraction pattern (Fig. 3c) shows a $[110]_{Fe}$ projection from bcc-iron and a $[110]_m$ projection from magnetite. The indexing of the diffraction patterns indicates that the unit cells of iron and magnetite are orientated in the same way, all three pairs of cube axes being parallel. The same orientational relationship between iron and magnetite was observed in the upper left part of Fig. 2a. This orientation relation can be written:

$$[100]_m \parallel [100]_{Fe}$$
$$[010]_m \parallel [010]_{Fe} \qquad \text{PLAIN STRUCTURE}$$
$$[001]_m \parallel [001]_{Fe}$$

The dark field image (Fig. 3b) was made from the 002_{Fe} reflection of iron and shows that iron having this orientation was present all over the image and quite evenly distributed. By moving the sample in the dark field mode we observed that the entire length of the thin edge of the magnetite grain contained iron of this orientation. A first approximation to a detailed description of smooth looking Plain Structure is thus as follows. Plain Structure showing no trace of hourglass patterns consists of a continuous network of bcc-iron partly covered by alumina-enriched magnetite and with pores having no preferred direction. All iron has the same crystallographic orientation as the original magnetite.

It should be emphasized that the above model may not give a complete description of all Plain Structure regions. We have indications that in Plain Structure showing hourglass patterns there are iron crystallites with other crystallographic orientations as well. There may be as many as 10 other crystallite orientations within these regions, but these findings have not yet been confirmed in independent specimens.

Finger structure. A structure related to Plain Structure is seen in Fig. 1g where the central parts of four Plain Structure grains contain particularly bright regions of various shapes and colours. This structure has been called Finger Structure because of the pointed fingers that make up the brightly coloured regions. Finger Structure displays the same partitioning of the former magnetite grains as does Plain Structure. This can be seen in the upper and lower grains of Fig. 1g, where bright yellow and purple regions seem to be located within corresponding lighter and darker Plain Structure triangles and trapezia. Finger Structure consists of 12 different variants of tapered fingers with a sheet-like pore structure. The fingers point along the four $\langle 111\rangle_m$ directions and are orthogonal to straight-lined grain boundary segments in Fig. 1g. Some regions in the reduced magnetite grains contain spots of three different colours. These are regions where three kinds of fingers are pointing along the same $\langle 111\rangle_m$ direction, which happens to be nearly orthogonal to the image plane, thus showing the fingers in cross section. We conclude that the fingers in three dimensions have a roughly circular cross section and are pointed like a pencil.

Judging from the colours of the fingers we see that the sheet-like pores within a finger have a component along the

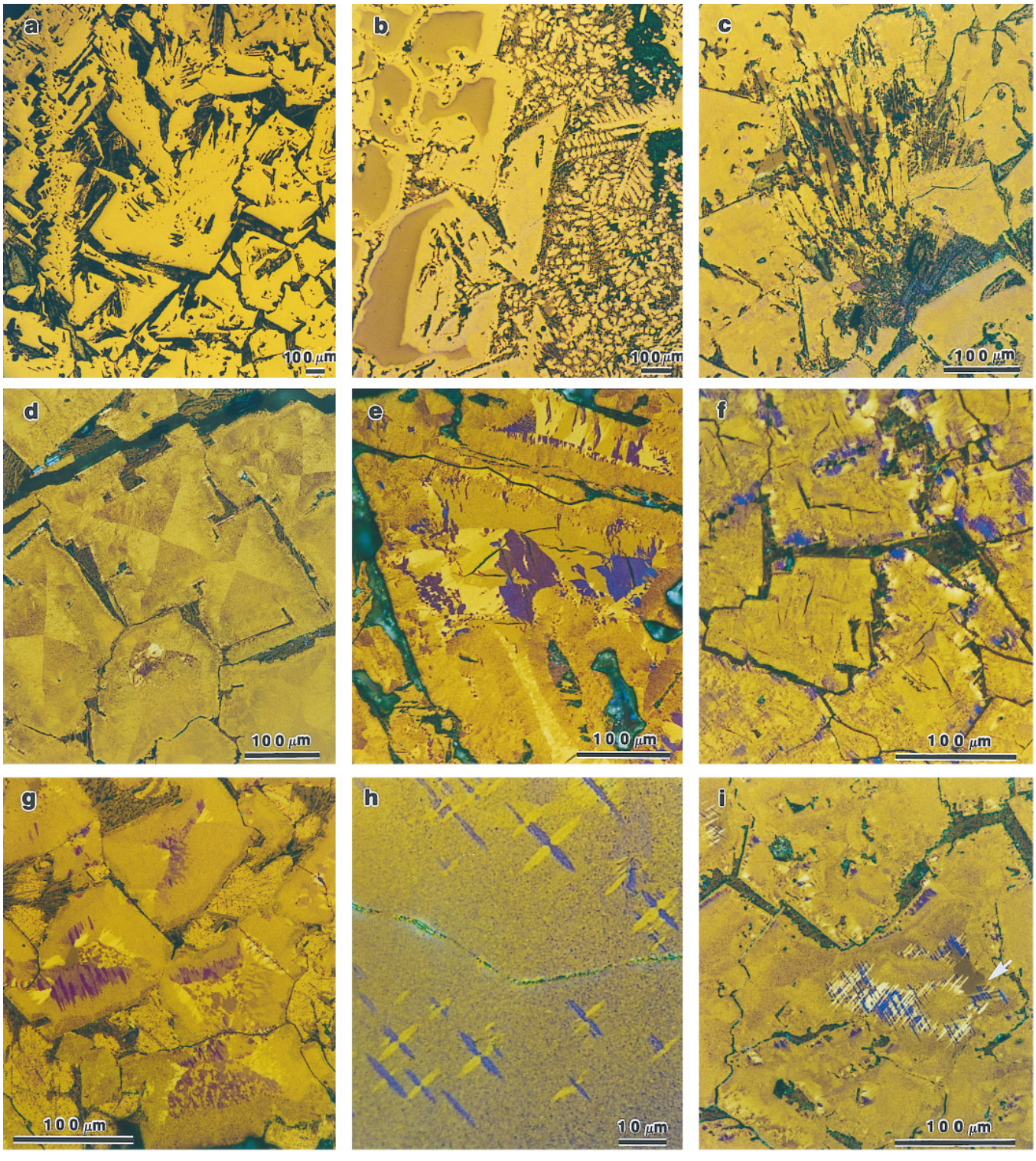

FIG. 1. Overview of structures in the industrial ammonia synthesis catalyst as seen in polarized light microscopy. (a) Dendritic magnetite with large, saw-tooth edged crystals. (b) Reduced wüstite having rounded dendrites that reduce easily compared to magnetite which remains in the central parts of the partly reduced grains at the left. (c) Needle-shaped oxide phases which contain iron and promoters like Al, K, and Ca. (d) Plain Structure, the most common of all, filling almost 80% of the catalyst volume. (e) Normal Structure, having large cracks in three brightly coloured regions. (f) Streaks and cracks parallel to the grain boundaries in grains with a low Fe^{2+} to Fe^{3+} ratio. (g) Finger Structure, with twelve kinds of fingers growing in the eight different $\langle 111 \rangle_m$ directions of each grain. (h) Cross Structure, made by unrestricted reduction, consisting of three mutually orthogonal discs of Normal Structure. (i) Flake Structure, with thin flakes containing sheet-like iron cutting deep into the residual magnetite.

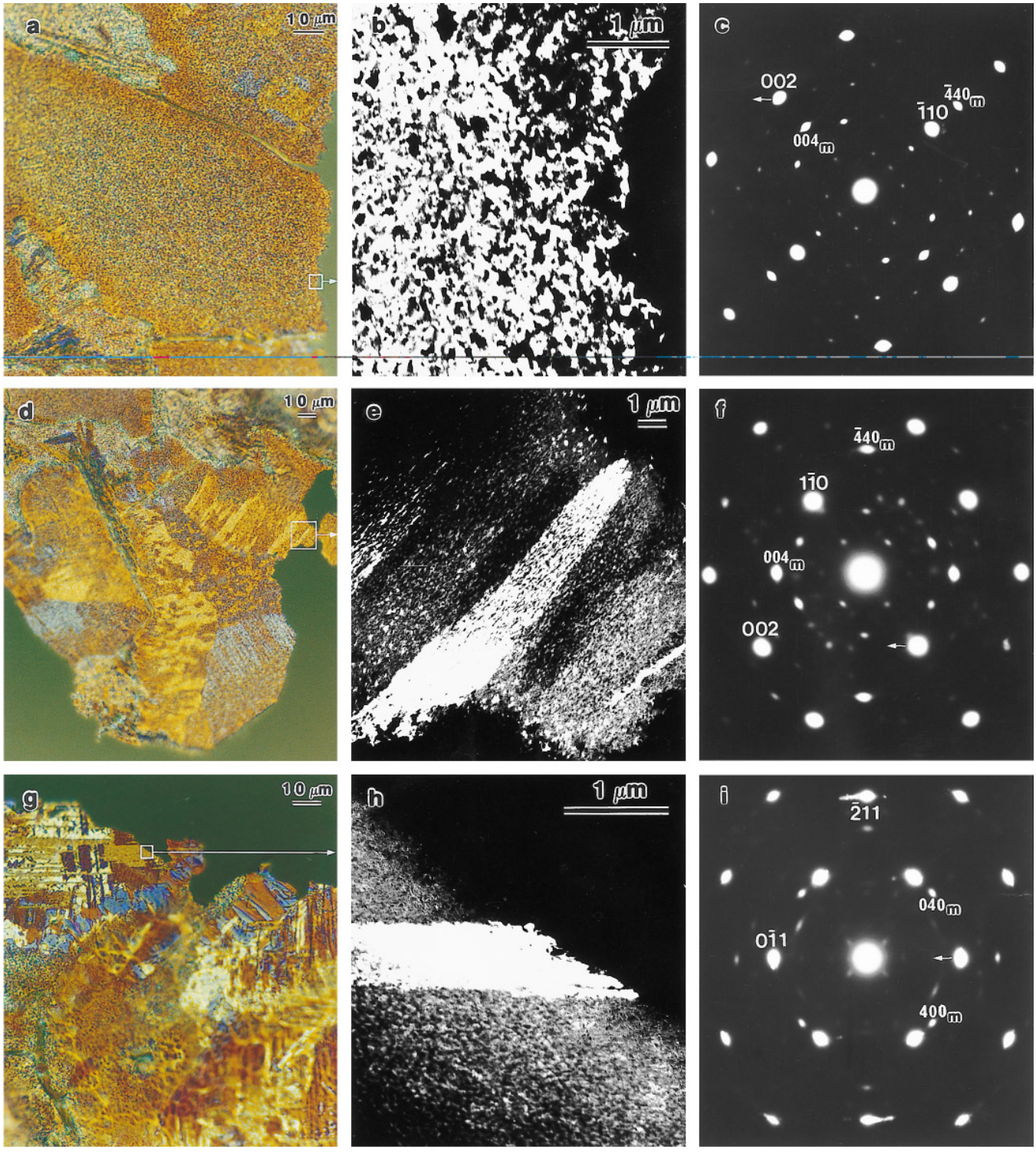

FIG. 3. TEM investigation of Plain Structure (a–c), Finger Structure (d–f), and Flake Structure (g–i). The left column contains optical micrographs of the TEM specimens that are shown as dark field images in the middle column. Corresponding diffraction patterns are given in the right hand column where small white arrows point left from the reflections used for dark field images. The patterns are indexed using large digits for bcc-iron and smaller digits with subscript m for magnetite reflections. All images within a row are orientated correctly relative to each other to facilitate orientational inferences.

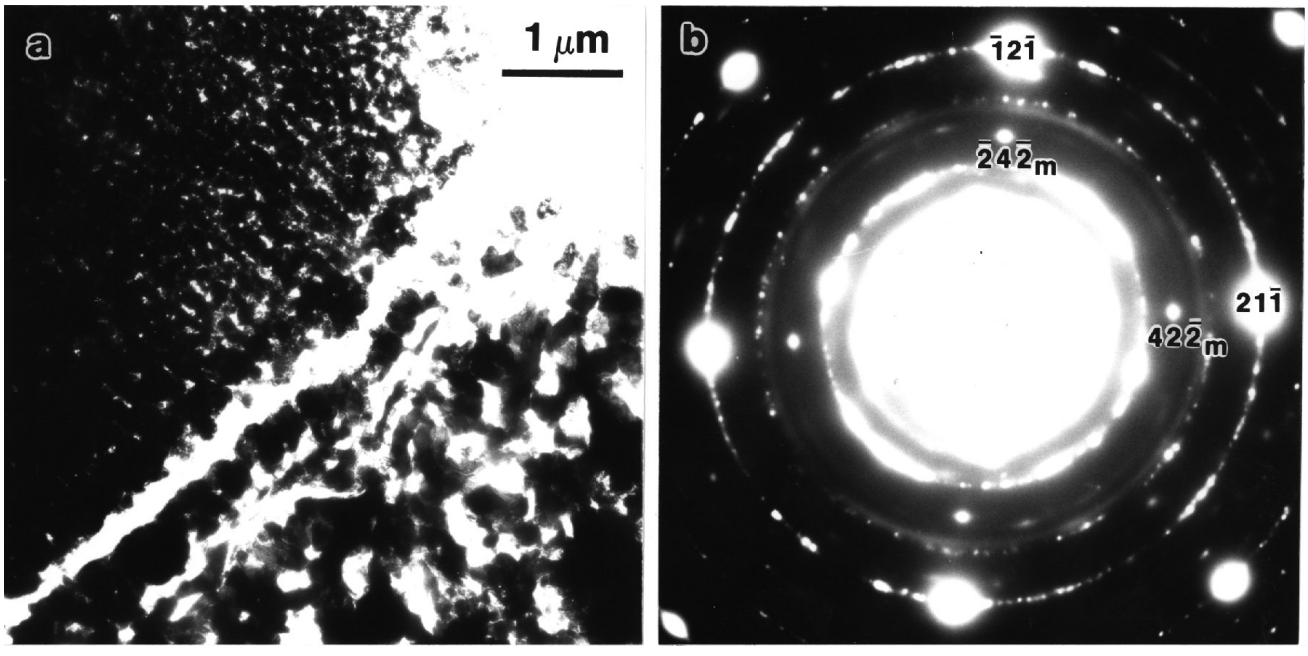

FIG. 2. Reduced wüstite in TEM. (a) Bright field image of interface between reduced magnetite (upper left) and reduced wüstite (lower right). (b) Diffraction pattern from the interface region containing a [135] projection of iron and magnetite from the upper left part and a polycrystalline ring pattern of iron from the reduced wüstite.

finger axis, i.e., along $\langle 111\rangle_m$. In this $\{111\}_m$ plane we expect threefold symmetry; hence it is not surprising that there are exactly three fingers for each of the four $\langle 111\rangle_m$ directions. Careful studies of several samples in optical microscopy and TEM have revealed that the sheet-like pores are parallel to $\{11\bar{2}\}_m$ planes. In a cubic system there are twelve non-equivalent $\{11\bar{2}\}_m$ planes, giving a unique pore orientation for each kind of finger.

In a magnetite grain with the shape of a perfect octahedron the eight octants, shaped like triangular-based pyramids, would contain three variants each of parallel fingers. Figure 4a shows three such fingers in one octant of a partly reduced magnetite grain. There are thus eight *signed* $\langle 111\rangle_m$ directions along which a finger can grow, all orthogonal to the outer grain surfaces. This geometry reflects the cubic symmetry of magnetite.

The special shape of the fingers seems to be a result of a nucleation and growth process during reduction. In a region reducing as Plain Structure the tip of a finger may form by some as yet unknown nucleation process. Once the tip has been formed, the finger starts to grow inwards and spreads out like a cone as reduction proceeds. The lateral expansion is halted when the finger meets a neighbouring finger. From there on they continue to grow along their common $\langle 111\rangle_m$ finger direction. The interface between residual magnetite and a single finger will often bulge slightly into the magnetite relative to the flat interface of the surrounding Plain Structure; see Fig. 4b. This indicates that Finger Structure reduces somewhat faster than Plain Structure. The opening angle of the finger tip cone gives information about the relative reduction rate of Plain and Finger Structure. Let us use a simplified model where the finger cone is considered to have cylindrical symmetry. Assuming a flat interface between magnetite and Plain Structure and a spherical interface at the base of the finger tip cone, it is straightforward to show that the relationship between the cone half angle α and the interface velocity ratio is $V_{\text{Plain}}/V_{\text{Finger}} = \cos\alpha$. Refer to Fig. 4b for details. Examination of an image where the fingers lay in the image plane gave a value for this ratio of 0.98 ± 0.01 based on eight finger tips, suggesting that Finger Structure grows between 1 and 3% faster than Plain Structure. This result seems reasonable since the sheet-like pores within the Finger Structure are such that they run orthogonally into the magnetite $\{111\}_m$ plane which is being reduced and the pores open a more direct way for the reduction gases to move in and out.

Figure 3d shows a reduced magnetite grain containing Finger Structure. The geometry is similar to the $(111)_m$ cut of Fig. 6g and we can see four regions with three variants of fingers in each region. We thus have all the 12 possible pore orientations in one image. Within the white box we see one individual finger that is more brightly yellow than the background. This finger lights up in Fig. 3e, showing that each finger consists of iron crystallites with one crystallographic orientation. The corresponding diffraction pattern in Fig. 3f shows a $[110]_{Fe}$ projection of bcc-iron and a $[110]_m$ projection from magnetite. In this case the projections are

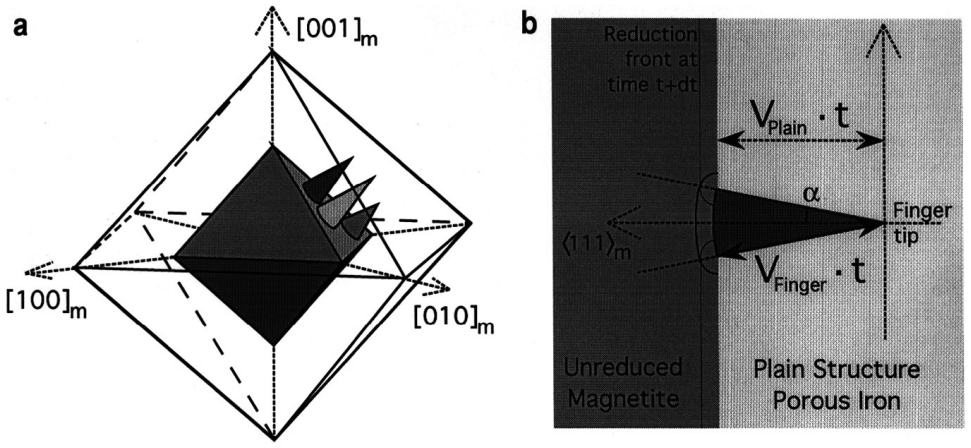

FIG. 4. The geometry of Finger Structure. (a) A partly reduced magnetite grain shaped like a regular octahedron. The porous iron is 'made transparent' and the smaller, solid octahedron in the centre symbolizes the unreduced core of magnetite. The three cube axes of magnetite are also drawn. Three conical fingers grow in the $[1\bar{1}\bar{1}]_m$ direction on the $(\bar{1}11)_m$ magnetite interface. In an ordinary grain of Finger Structure, the fingers would grow in all of the possible eight signed $\langle 111\rangle_m$ directions. (b) A simple model for finger growth. The finger was nucleated at the origin of the dotted coordinate system and started growing in the $\langle 111\rangle_m$ direction at time $t=0$ with velocity V_{Finger} which was slightly larger than the velocity, V_{Plain}, of the interface between magnetite and Plain Structure. At time t the finger has the shape of a cone with a spherical base of radius $V_{\text{Finger}} \cdot t$ whereas the Plain Structure interface has moved a distance $V_{\text{Plain}} \cdot t$. Trigonometry gives the relation $\cos\alpha = V_{\text{Plain}}/V_{\text{Finger}}$, where α is the half angle of the cone. The thin solid lines drawn in the magnetite show the hypothetical reduction front after a time $t+dt$ if either only the Plain Structure or only the finger were allowed to reduce and spread in all directions during the time interval dt. The crossing point of the two fronts lies on the extension of the cone into the magnetite, showing that the finger cone will retain its shape as long as the ratio of the reduction velocities remains constant.

rotated 35° relative to each other about their common [110] direction. This makes $[1\bar{1}2]_{Fe}$ parallel to $[004]_m$ and $[2\bar{2}2]_{Fe}$ parallel to $[\bar{4}40]_m$ as can be seen from the indexed patterns. After some straightforward vector calculations we obtain the orientation relations

$$\begin{aligned} [100]_m &\parallel [\sqrt{6}-2,\ \sqrt{6}+2,\ 2]_{Fe} \\ [010]_m &\parallel [\sqrt{6}+2,\ \sqrt{6}-2,\ -2]_{Fe} \\ [001]_m &\parallel [2,\ -2,\ 4]_{Fe} \end{aligned} \quad \text{FINGER STRUCTURE}$$

where the Fe vectors all have length $2\sqrt{6}$. The 12 other coordinate systems describing the orientation of iron in the other fingers may be generated from the one above by applying suitable cyclic permutations and sign changes of the coordinates of the iron vectors. This is equivalent to performing threefold rotations about the $\langle 111\rangle_m$ axes and fourfold rotations about the $\langle 100\rangle_m$ axes, respectively, in accordance with the cubic symmetry of the system. If we interpret the 9 coordinates of the iron vectors as a 3 by 3 matrix, these symmetry operations can be performed by matrix multiplication. We will not go into the details of this process here. We note, however, that all the iron crystallites end up having a $\langle 2\bar{2}1\rangle_{Fe}$ direction parallel to the 12 different $\langle 11\bar{2}\rangle_m$ directions of magnetite, which are normal to the weakly sheet-like pores in Finger Structure. Further, within the plane of the sheets a $\langle \bar{1}14\rangle_{Fe}$ direction of iron is parallel to the finger axis, i.e., a $\langle 111\rangle_m$ direction. Also within the sheets and normal to this, a $\langle 110\rangle_{Fe}$ direction of iron is parallel to a $\langle \bar{1}10\rangle_m$ direction of magnetite, giving rise to the common $\langle 110\rangle$ projection. These orientation relations can be confirmed by comparing Figs. 3e and 3f. This finger grew in the $[1\bar{1}1]_m$ direction with the pores normal to $[\bar{1}12]_m$. We thus view the pores edge on, and that is why this finger has the brightest yellow colour in the optical micrograph (Fig. 3d).

Normal structure. Figure 1e shows a grain containing what we call Normal Structure. This structure was described thoroughly in Ref. (13) but the term Normal Structure was not used there. We include it here for reasons of completeness. Normal Structure is characterized by regions of bright colours with no particular shape but occasionally containing straight-line cracks. Three regions of different colours appear within one reduced magnetite grain. Each region contains sheets of iron stacked side by side and the large cracks are parallel to the sheets. In Fig. 1e, a triangle is formed by one crack in each of the three regions—yellow, purple, and smooth, light brown. The three regions are symmetry equivalent and the iron sheets are parallel to each of the three $\{100\}_m$ planes in the original magnetite grain. All the sheets in one coloured region are parallel and have the same crystallographic orientation, namely a $\langle 100\rangle_{Fe}$ direction along the sheet normal, i.e., parallel to the $\langle 100\rangle_m$ direction of magnetite. The $\langle 010\rangle_{Fe}$ and $\langle 001\rangle_{Fe}$ axes of iron are parallel to the $\langle 011\rangle_m$ and $\langle 0\bar{1}1\rangle_m$ directions, respectively. One reason for calling the structure of Fig. 1e Normal Structure is that the orientational relationship given above is the normal, well established epitaxy relation when bcc-iron is oxidized to magnetite (23, 24). Further, the iron sheets in

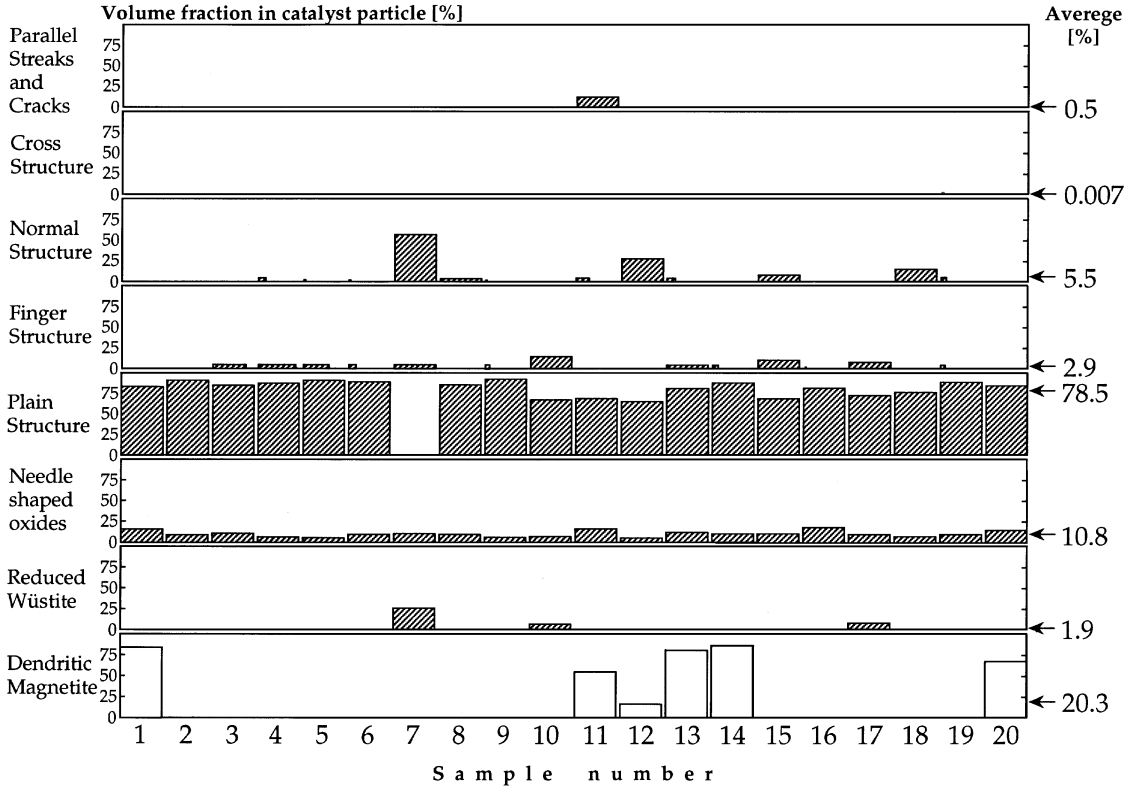

FIG. 5. Quantitative statistics of industrial ammonia synthesis catalyst. This figure shows the relative amounts of structures and phases in twenty randomly selected catalyst particles numbered 1 to 20 on the horizontal axis. Since dendritic magnetite itself contains structures, it was not included in the total area when percentages were calculated. Assuming the equivalence of area fractions and volume fraction in our samples, the average values at the right should give an estimate of the relative abundance of the various structures in the samples of catalyst A examined in this study. In order to show accurately the smallest volume fractions, the rectangles were shortened horizontally. Thus the percentage numbers on the left hand vertical axis apply only to volume fractions larger than 5%.

the three kinds of regions are mutually orthogonal, or *normal*, to each other.

In Ref. (13) we further showed that the Normal Structure regions contained large scale magnetic domains with in-plane magnetization within the iron sheets. We have not found evidence for similar magnetic domains in any of the other structures described here.

Cross structure. A special kind of Normal Structure is shown in Fig. 1h and has been given the name Cross Structure or Crosses for short. The Crosses consist of porous iron with a Normal Structure type of iron sheet and crystallographic orientation. In three dimensions a Cross is made up of three mutually orthogonal, interpenetrating discs, each containing one kind of Normal Structure sheet. The cross shape appears when two of the discs are seen edge on in the polishing plane and the third disc lies either above or below this plane. We have indications that Crosses form along narrow cracks in the magnetite where reduction starts at one point, e.g., a dislocation crossing the plane of the crack. The reduction gases can enter and escape through the crack and the reduction is free to proceed in all directions. The resulting three-dimensional shape of the Cross should give important clues regarding the anisotropy and general nature of the Normal Structure reduction process. Measurements on the individual arms of the seven Crosses in Fig. 1h give a length/width ratio of 7 ± 2, suggesting that the disc grows between five and nine times faster in the plane of the disc than normal to it. As was the case for Finger Structure, it seems that a structure having sheets that run orthogonally into the magnetite tends to grow most rapidly. Again the reason could be the easy transport of gas to and from the interface, but it is likely that many other factors like local stress and strain, iron–magnetite epitaxy relations, diffusion mechanisms, defect structure, temperature, pressure, reduction gas composition, etc., would have to be considered in a complete model of the reduction process of any given structure.

Bright streaks and cracks along $\{111\}_m$ planes of magnetite. The structure in Fig. 1f contains both large cracks and bright colours, but is distinctly different from Normal Structure. Here the brightly coloured regions are not smooth and they are generally located close to the grain boundaries and not in the interior of the former magnetite grain. Looking at the large cracks in the grain at the lower

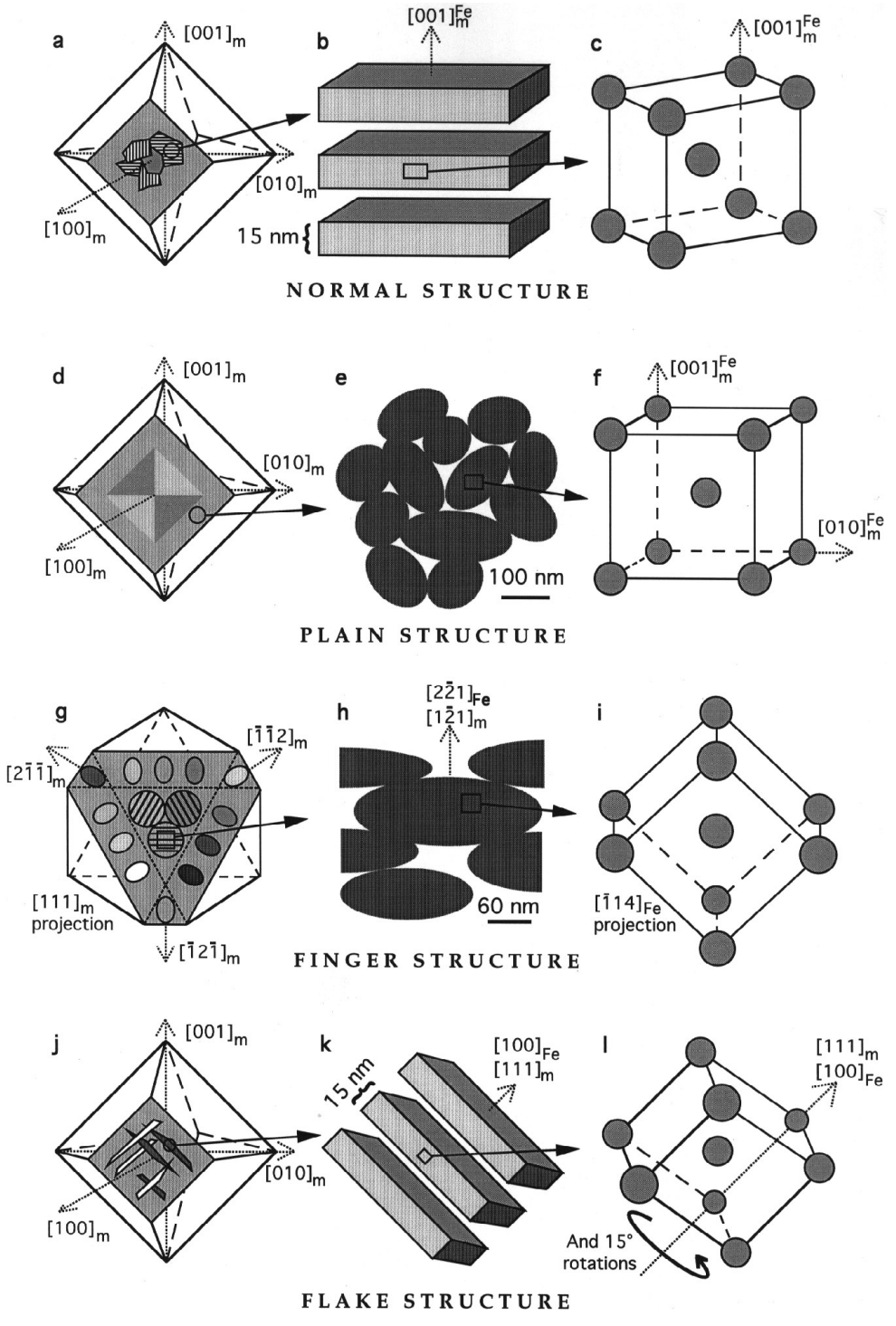

FIG. 6. Summary of the four structures found within reduced magnetite grains. The left column shows magnetite grains shaped like regular octahedra which have been ground and polished like a metallographic sample to reveal the various structures in the grey-shaded polishing plane. The middle column contains schematic drawings of the local pore structure from the selected regions shown by arrows from the left column. The body centred unit cells of α-Fe in the right hand column show the crystallographic orientation of iron in regions with the given pore structure.

left of Fig. 1f, one will notice that the cracks are parallel to straight segments of the grain boundary and can thus be assumed to lie along the $\{111\}_m$ planes of magnetite. In accordance with this, no more than four different crack directions are observed in this and similar grains.

This structure of bright stripes and cracks parallel to $\{111\}_m$ was very common in the reduced particles of catalyst C and was the only structure in addition to needle-shaped oxide phases which we observed in those specimens. The absence of reduced wüstite in the samples of catalyst C and in regions such as Fig. 1f indicates that the Fe^{2+} to Fe^{3+} ratio in the unreduced particles is close to or below 0.5. Our optical microscope observations of this particular structure agree well with the results of Pennock *et al.* (3). They reported large channels and 20–30 nm pores along $\{111\}_m$ planes, such channels being visible in Fig. 1f as dark cracks and the pores as regions of bright colours.

Flake structure. Another structure having sheets of iron along $\{111\}_m$ planes is the one shown in Fig. 1i. Here, brightly coloured flakes of porous iron are seen cutting through each other in the interior of a partly reduced magnetite grain. The flakes appear as needles where they cross the polishing plane and exactly four different orientations of needles can be found in this image: The yellow and blue are quite obvious and two light brown needles of different orientation can be seen within the unreduced magnetite at the tip of the white arrow. The needles are parallel to straight segments of the original grain boundary.

The Flake Structure contains parallel sheets of iron that lie along the four $\{111\}_m$ planes of magnetite within each flake. The flakes grow very characteristically by individually cutting deep into the magnetite as shown in Fig. 1i. A survey of a grain similar to the one in this figure but at larger magnification gave a length to width ratio for the blue and yellow needles of 21 ± 7. This is significantly more than for Crosses and shows that the reduction velocity along the $\{111\}_m$ plane is roughly 20 times faster than normal to the plane.

Flake Structure is extremely rare in the industrially prereduced catalyst and has been observed in only one such particle of the more than 250 studied so far. However, in laboratory-reduced particles where pure H_2 was used as reduction gas, Flake Structure was one of the most common structures. It may be that the presence of N_2 during reduction will somehow prevent nucleation of the flakes, or promote other structures.

Figure 3g shows a TEM sample containing both Normal Structure and Flake Structure at the thin edge. This sample has proved useful in determining the orientation relations of Flake Structure and establishing that it is indeed different from Normal Structure. The three Normal Structure regions appear light yellow, blue–gray, and brown in this micrograph. Three Flake Structure regions are seen at the upper left and appear in light brown and two dark shades of brown. The white box is placed on one of the light brown flakes. In the dark field image of Fig. 3h an iron region in the central part of the image lights up even though the entire image was made within the evenly coloured flake of Fig. 3g. This shows that in Flake Structure, there is not a one-to-one correspondence between pore orientation and iron orientation as in Normal and Finger Structure. This degeneration results from the fact that there are only four $\{111\}_m$ planes along which the flakes can run whereas there are as many as 24 different crystallographic orientations of iron in Flake Structure. The large number of possible iron orientations within one reduced magnetite grain has been deduced from images like Fig. 3i and from symmetry considerations. In the selected area diffraction pattern of Fig. 3i we see a $[111]_{Fe}$ projection of iron and a $[001]_m$ projection of magnetite. From this we obtain the orientational relationships

$$\begin{aligned} [100]_m &\parallel [2, \quad \sqrt{3}-1, -\sqrt{3}-1]_{Fe} \\ [010]_m &\parallel [-2, \sqrt{3}+1, -\sqrt{3}+1]_{Fe} \\ [001]_m &\parallel [2, \quad 2, \qquad 2]_{Fe} \end{aligned} \qquad \text{FLAKE STRUCTURE}$$

where the iron vectors all have length $2\sqrt{3}$. Applying the cubic symmetry elements on this orientation relation will generate 12 nonequivalent coordinate systems describing the orientation of iron crystallites. These 12 systems can be arranged into four groups where the three systems in each group have a common $[100]_{Fe}$ axis parallel to one of the four $\langle 111\rangle_m$ axes of magnetite. Within the $\{111\}_m$ plane these three systems are related by a 120° rotation. It turns out that the sheets of iron within the flakes all have a $[100]_{Fe}$ axis normal to the sheets. As can be seen from Fig. 3h, sheets of iron with the same crystallographic orientation are stacked together parallel to each other within the flake. In this particular image the individual sheets overlap and appear blurred since we see the sheets at a 55° angle. The sheet normal is here along $[100]_{Fe}$ which is parallel to $[1\bar{1}1]_m$. The grey regions above and below the white part of Fig. 3h are also sheets of iron parallel to $(1\bar{1}1)_m$ but contain iron of the kinds rotated by ±120° about the $[1\bar{1}1]_m$ sheet normal. These two kinds of iron have their $[111]_{Fe}$ axes along $[100]_m$ or $[010]_m$, and have irrational projections along $[001]_m$ thus giving no contribution to the diffraction pattern of Fig. 3i.

To complicate matters further, we have diffraction evidence that there are 12 other possible orientations of iron in the Flake Structure. The easiest way of describing them is to say that one can obtain these 12 systems by a 15° rotation of each of the previously described Flake systems about the sheet normals $[100]_{Fe}$ which are parallel to $\langle 111\rangle_m$. Detailed studies of diffraction patterns indicate that two of the latter kinds of systems tend to be associated with one of the former. For instance, in Fig. 3i there are 'satellite reflections' on each side of the $\bar{2}11_{Fe}$ and $2\bar{1}\bar{1}_{Fe}$ reflections. The positions of these spots are consistent with

the assumption that two kinds of iron of the latter type are present in the white flake of Fig. 3h. These two iron systems do not have a proper projection along $[001]_m$ but rather $\langle 1/\sqrt{3}\ \sqrt{2}/\sqrt{3}\ 1/\sqrt{2}\rangle_{Fe}$ projections giving systematic rows of 211_{Fe} reflections 8.6° to the left and right of the $\bar{2}11_{Fe}$ reflection of Fig. 3i. We have not studied the detailed crystallite distribution of these three iron orientations within the white Flake region of Fig. 3h. However, it seems that the one kind of iron described first dominates, and that there are generally small amounts of the two other kinds of iron present along with it. It is interesting to note that in any case the pore structure of the Flake and Normal Structures are locally very similar, namely roughly 15 nm thick sheets of bcc-iron with a $\langle 100\rangle_{Fe}$ direction of iron normal to the sheets.

All the orientational relations given here should be understood as idealizations describing average positions. There is always a certain spread in the crystallite orientation distribution about any particular direction. It is not surprising that a porous system like this catalyst allows slight rotations and bending of the iron out of its ideal orientation.

Measurement of Surface Resistance in the Various Structures

We performed an experiment in order to study the connectivity of the porous iron and oxides. Some authors describe the catalyst as porous single crystals of iron (12), whereas others seem to speak of isolated iron crystallites more or less covered by oxides (4, 17).

By positioning two needles precisely at the desired places on the surface of optical microscope specimens we were able to obtain values for the electrical resistance in the surface of the various structures. If the crystallites were electrically isolated, e.g. by a layer of magnetite, the resistance should be comparable to that of magnetite. If, on the other hand, the catalyst consisted of a more or less continuous network of iron with oxides covering only the surface, the resistance should be comparable to that of iron.

We made measurements on samples containing the various structures and used surfaces of steel, silver, and platinum as references. Steel gave a reading of 0.6 Ω, silver 0.4 Ω, platinum 0.3 Ω and the connecting leads alone 0.1 Ω. Since iron and platinum have about the same resistivity (10 and 11×10^{-8} Ω m, respectively) and pure silver has about one seventh of this value (1.6×10^{-8} Ω m) our measurements indicate that the oxide covering is also important, assuming that Pt was least oxidized. The value for steel is the same as the reading we obtained when both needles were placed within iron sheets of Normal Structure where the sheets were parallel to the polished surface. In other Normal Structure regions the reading was 2 Ω. In Plain structure regions we obtained stable readings of 1 Ω and in reduced wüstite 1.5 Ω. In comparison, unreduced magnetite gave readings of about 60 Ω or higher. This strongly indicates that the iron crystallites are electrically connected both in reduced wüstite and in reduced magnetite. In regions where all the iron is found to have the same crystallographic orientation it is thus meaningful to speak of porous single crystals of iron even though these crystals contain oxide phases on their inner surfaces and the crystallographic details of the iron sheet touching points are not known.

The reduced needle-shaped phases gave readings of about 35 Ω whereas the *unreduced* needle shaped phases had a resistance about 2000 times higher, showing that these oxides are true insulators.

Statistics on Relative Abundance of the Various Structures

Figure 5 shows the results of the quantitative examination of 20 randomly selected particles from industrially reduced specimens of catalyst A. The horizontal axis lists the 20 samples studied. The structures described above are represented vertically with the exception of Flake Structure which was not found among the 20 particles. The rectangles show the relative abundance of a structure within each catalyst particle. Since Dendritic Magnetite always contains other structures, the area of dendritic magnetite was not included when calculating the total area of each particle because this area had already been accounted for by other structures, typically Plain Structure. Hence, the area of rectangles for each sample excluding dendritic magnetite adds up to 100%. The numbers in the right hand column are the total area of each structure divided by the total segmented area. This should give an estimate of the average volume fraction of the structures. However, we clearly see that the variance in the data is very large, reflecting the great inhomogeneity of the catalyst. For instance, in sample number 7 nearly all reduced magnetite consisted of Normal Structure whereas the rest of the particle was largely reduced wüstite.

DISCUSSION

After arriving at this fairly detailed description of the catalyst, several interesting questions arise. Apart from questions regarding the specific catalytic activity of the various structures, there are more fundamental questions such as: Why does magnetite reduce in so many different ways? What is the mechanism of reduction in each case? We have previously mentioned some of the factors that may influence the mechanism of reduction and will take up here just one of them in a qualitative argument based on epitaxy and lattice matching.

Looking at the lattice constants of iron, $a_{Fe} = 0.287$ nm, and magnetite, $a_m = 0.840$ nm, it turns out that $\sqrt{8}\, a_{Fe}/a_m = 0.966$ while $3\ a_{Fe}/a_m = 1.024$, which gives the lattice mismatch for the Normal Structure and Plain Structure orientations, respectively. Thus the magnetite unit cell is too small to match perfectly with Plain Structure and too large to match perfectly with Normal Structure. By adjusting the lattice parameter of the magnetite phase one would expect

to be able to obtain a better matching that would increase the likelihood of one of these two structures relative to the other. Alumina, Al_2O_3, dissolved in magnetite is known to reduce the lattice parameter linearly with concentration (4, 25). This means that an increase in the alumina content will reduce the mismatch between Normal Structure and the magnetite phase, but increase the mismatch with Plain Structure. One might therefore assume that reduction of a grain with an alumina content below a certain limit would yield Plain Structure, whereas Normal Structure would result if the alumina content was above this limit.

Despite their different orientations relative to the original magnetite, the local geometry of Flake and Normal Structure is similar in the sense that we observe iron sheets with $\{100\}_{Fe}$ surfaces in both cases. In contrast, Finger Structure has a $\langle 221\rangle_{Fe}$ direction of iron orthogonal to the sheets, whereas there seems to be no particular low index plane bordering the iron crystallites in Plain Structure. Although this study indicates that the presence of $\{100\}_{Fe}$ and $\{221\}_{Fe}$ surface planes of iron *on average* in Normal/Flake and Finger Structures, respectively, stepped surfaces or small scale surface restructuring (26) might be widespread, exposing other iron facets to the synthesis gas in the active catalyst.

Potassium has been shown to eliminate the difference in activity for various low index iron surfaces (27). Thus, with or without steps or restructuring, there might not be any significant difference in activity per unit surface area of iron in the different structures. However, the surface area per volume, or per mass, might vary among the structures. If, for instance, the random pores of Plain Structure give a surface area per volume which is different from Normal Structure, the activity per catalyst volume may be different. Since this present study describes the nanometer scale pore structure and does not assess the surface area of the different structures, it is premature at this time to draw conclusions regarding the connection between catalytic activity and the structures described here.

CONCLUSION

We have studied the same specimens of industrial ammonia synthesis catalyst in both optical microscopy and transmission electron microscopy. The catalyst is a very inhomogeneous system containing several phases and different kinds of pore structure. Reduced wüstite has relatively large pores and a random distribution of iron crystallites. Reduced magnetite displays at least four distinctly different kinds of structure with characteristic shape, pore geometry and crystallographic orientation of the porous iron. A spinel type oxide phase is present in the stabilized catalyst and this alumina-enriched magnetite phase has the same crystallographic orientation as the original magnetite. Figure 6 shows a schematic summary of the four different structures found in reduced magnetite grains, referred to as Normal Structure, Plain Structure, Finger Structure and Flake Structure, respectively.

The surface area might differ between the structures. Thus, even with similar catalytic activity per unit surface area in the four structures, there could still be differences in activity per volume.

ACKNOWLEDGMENTS

The author would like to thank Norsk Hydro A/S for active technical support and for helpful discussions in the preparation of this article. I am also grateful to Professor Johan Taftø for his continuous encouragement during the research process and for reading through the various versions of the manuscript. This project was sponsored by the Norwegian Research Council (Norges Forskningsråd) and their contribution is gratefully acknowledged.

REFERENCES

1. Schäfer, K., *Z. Electrochem.* **64**, No. 10, 1190 (1960).
2. Rayment, T., Schlögl, R., and Thomas, J. M., *Nature* **315**, 311 (1985).
3. Pennock, G. M., Flower, H. M., and Andrew, S. P. S., *J. Catal.* **103**, 1 (1987).
4. Schlögl, R., *in* "Catalytic Ammonia Synthesis" (J. R. Jennings, Ed.), p. 19. Plenum, New York, 1991.
5. Peters, CL., Schäfer, K., and Krabetz, R., *Z. Elektrochem.* **64**, 1194 (1960). [In German]
6. Menon, P. G., and Skaugset, P., *Appl. Catal. A* **115**, 295 (1994).
7. Sasa, Y., Uda, M., and Toyoshima, I., *Chem. Lett.* 2011 (1982).
8. Clausen, B. S., Mørup, S., Topsøe, H., Candia, R., Jensen, E. J., Baranski, A., and Pattek, A., *J. Phys. Colloq. C6* **37**, 245 (1976).
9. Borghard, W. S., and Boudart, M., *J. Catal.* **80**, 194 (1983).
10. Pattek-Janczyk, A., and Miczko, B., *Solid State Ionics* **38**, 171 (1990).
11. Fastrup, B., Muhler, M., Nygård Nielsen, H., and Pleth Nielsen, L., *J. Catal.* **142**, 135 (1993).
12. Taftø, J., Kristiansen, L. A., and Fuglerud, T., *Phil. Mag. Lett.* **64**, 105 (1991).
13. Holme, B., and Taftø, J., *J. Catal.* **152**, 243 (1995).
14. Lyman, T., "Metals Handbook Vol. 8," American Society for Metals, 8th ed. 1973.
15. Pattek-Janczyk, A., Hrynkiewicz, A. Z., Kraczka, J., and Kulgawczuk, D., *Appl. Catal.* **6**, 35 (1983).
16. Baranski, A., Lagan, M., Pattek, A., Reizer, A., Christiansen, L. J., and Topsøe, H., *in* "Preparation of Catalysts," Vol. 2, p. 353. Elsevier, Amsterdam, 1979.
17. Nielsen, A., *Catal. Rev.–Sci. Eng.* **23**, 17 (1981).
18. Jensen, E. J., Topsøe, H., Sørensen, O., Krag, F., Candia, R., Clausen, B. S., and Mørup, S., *Scand. J. Metall.* **6**, 6 (1977).
19. Pattek-Janczyk, A., Baranski, A., Kotarba, A., Kowalska, A., Miczko, B., Pyrczak, E., Reizer, A., Reubenbauer, K., Sepiol, B., and Spiewak, Z., *Appl. Catal.* **39**, 169 (1988).
20. Pernicone, N., and Traina, F., *in* "Preparation of Catalysts," Vol. 2, p. 321. Elsevier, Amsterdam, 1979.
21. Holme, B., *in* "Structures in the Porous Iron Ammonia Synthesis Catalyst." M.S. Thesis, University of Oslo, 1992.
22. Dry, M. E., and Ferreira, L. C., *J. Catal.* **7**, 352 (1967).
23. Mehl, R. F., McCandless, E. L., and Rhines, F. N., *Nature* **134**, 1009 (1934).
24. Mehl, R. F., and McCandless, E. L., *Nature* **137**, 702 (1936).
25. Westrik, R., *J. Chem. Phys.* **21**, 2094 (1953).
26. Strongin, D. R., and Somorjai, G. A., *J. Catal.* **118**, 99 (1989).
27. Strongin, D. R., and Somorjai, G. A., *in* "Catalytic Ammonia Synthesis" (J. R. Jennings, Ed.), p. 144. Plenum, New York, 1991.